

Specific Role of Potassium in Promoting Ag/Al₂O₃ for Catalytic Oxidation of Formaldehyde at Low Temperature

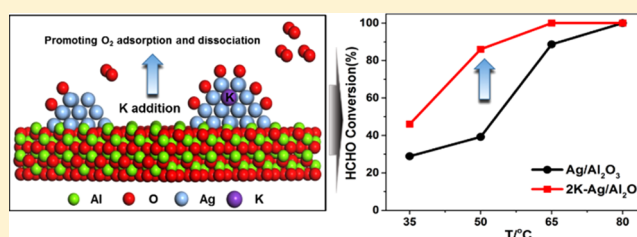
Xueyan Chen,^{†,‡} Min Chen,^{†,‡} Guangzhi He,^{†,‡,Ⓜ} Fei Wang,^{†,‡,Ⓜ} Guangyan Xu,^{†,‡,Ⓜ} Yaobin Li,^{‡,§} Changbin Zhang,^{*,†,‡,Ⓜ} and Hong He^{†,‡,§}

[†]State Key Joint Laboratory of Environment Simulation and Pollution Control, Research Center for Eco-Environmental Sciences, Chinese Academy of Sciences, Beijing 100085, China

[‡]University of Chinese Academy of Sciences, Beijing 100049, China

[§]Center for Excellence in Regional Atmospheric Environment, Institute of Urban Environment, Chinese Academy of Sciences, Xiamen 361021, China

ABSTRACT: Ag-based catalysts are efficient materials for formaldehyde (HCHO) oxidation in the low-temperature range. It has been reported that K addition can increase the catalytic performance of Ag-based catalysts, whereas the specific role of K doping remains ambiguous. In this work, Ag/Al₂O₃ and K–Ag/Al₂O₃ catalysts with different K doping levels were prepared and subsequently tested for catalytic HCHO oxidation. It was observed that K doping has a dramatic promotion effect on the activity of the Ag/Al₂O₃ catalyst. The 2K–Ag/Al₂O₃ sample was the most active catalyst, over which HCHO could be completely converted into CO₂ and H₂O in a gas hourly space velocity of 100 000 mL/(g_{cat} h) at 65 °C. The catalysts were next characterized by X-ray powder diffraction, Brunauer–Emmett–Teller, transmission electron microscopy, H₂-temperature-programmed reduction, UV–vis, X-ray absorption fine structure, and in situ diffuse reflectance infrared Fourier transform spectroscopy methods. The characterization results show that addition of K species increased the content of metallic Ag species in Ag/Al₂O₃ catalysts and promoted the adsorption and activation of oxygen species, whereas excessive doping with K⁺ resulted in the agglomeration of Ag particles and loss of some metallic sites. Therefore, the 2K–Ag/Al₂O₃ catalyst demonstrated the best performance among the series of K-doped catalysts. Promotion of O₂ activation by K doping, rather than enhanced Ag dispersion or surface OH activation or exposure of more Ag(111) facets, was found to be the key factor in the improved catalytic performance of K–Ag/Al₂O₃ catalysts.



INTRODUCTION

Formaldehyde (HCHO) is one of the major indoor air contaminants, leading to serious hazards to human health.^{1–4} Therefore, it is of great importance to effectively abate indoor air HCHO. Over the past decades, four kinds of methods based on adsorption, photocatalysis, plasma technology, and catalytic oxidation have attracted the attention of researchers for the removal of HCHO.^{5–9} Among them, catalytic oxidation is regarded as the most promising method due to its high effectiveness in achieving total conversion of HCHO into harmless CO₂ and water.¹⁰

Currently, the conventional catalysts used in the catalytic oxidation of HCHO include transition-metal oxides (Co, Cu, Ce, and Mn)^{11–17} and supported precious metal (Pt, Pd, Au, and Ag) catalysts.^{18–39} In general, the supported noble-metal catalysts such as Pt-, Pd-, and Au-based catalysts exhibit excellent activity for HCHO oxidation at ambient temperature even at high space velocity, whereas the transition-metal oxides need much higher temperatures to achieve complete combustion of HCHO. However, wide application of Pt, Au, and Pd is limited by their high cost, thus accelerating the flourishing of studies on Ag-based catalysts. Ag-based catalysts

are much less expensive and show considerable efficiency for HCHO oxidation at low temperature. A recent study reported that a 1.7K–Ag/Co₃O₄ catalyst can reach 100% HCHO conversion at 70 °C.²⁶

Previously, we have demonstrated that the addition of alkali metal ions (such as Li⁺, Na⁺, and K⁺) on Pt/TiO₂ catalysts can dramatically promote the catalytic efficiency for HCHO by inducing and stabilizing the atomically dispersed Pt species.⁴⁰ Then, we further proved that this promotion effect of alkali metal ions on Pt catalysts can also be applied to Pd-based catalysts.²² In contrast, the effects of alkali ions on Ag-based catalysts are rarely investigated to date. Recently, Bai et al.²⁶ prepared Ag/Co₃O₄ and K–Ag/Co₃O₄ catalysts using three-dimensional ordered mesoporous Co₃O₄ as support and observed that K addition markedly promoted the catalytic performance of Ag/Co₃O₄ for HCHO oxidation. The promotion effect of K⁺ species has been attributed to the creation of more abundant surface OH species, active Ag(111)

Received: July 25, 2018

Revised: October 8, 2018

Published: November 9, 2018

Table 1. Contents of Ag and K and Physical Parameter of Ag/Al₂O₃ and K-doped Ag/Al₂O₃ catalysts

samples	content (wt %)		S_{BET} (m ² /g)	pore volume (mL/g)	pore diameter (nm)
	Ag	K			
γ -Al ₂ O ₃			187.8	1.00	17.9
Ag/Al ₂ O ₃	8.05		146.7	0.577	17.8
0.5K-Ag/Al ₂ O ₃	7.93	0.37	134.7	0.688	17.8
1K-Ag/Al ₂ O ₃	7.59	0.93	130.1	0.728	18.0
2K-Ag/Al ₂ O ₃	7.77	1.84	127.9	0.724	17.9
4K-Ag/Al ₂ O ₃	7.65	3.76	135.0	0.646	17.9

facets, Co³⁺ ions, and O²⁻ species on K-Ag/Co₃O₄ catalysts. It is clear that the changes induced by K addition to Ag/Co₃O₄ are very complicated because the reducible support Co₃O₄ was employed and the specific role of K still remains ambiguous.

Al₂O₃ is a stable and nonreducible support, and generally not directly involved in the catalytic reaction. Therefore, in this study, we prepared Ag/Al₂O₃ and K-Ag/Al₂O₃ catalysts to investigate how K addition affects the performance of Ag-based catalysts in HCHO oxidation. The series of catalysts was tested and the results verified that K addition also had a dramatic promotion effect on the Ag/Al₂O₃ catalyst. The 2K-Ag/Al₂O₃ sample, which could completely oxidize 110 ppm of HCHO to CO₂ and H₂O at 65 °C with a gas hourly space velocity of 100 000 mL/(g_{cat} h), showed the best catalytic performance. The catalysts were next characterized by X-ray powder diffraction (XRD), Brunauer–Emmett–Teller (BET), transmission electron microscopy (TEM), H₂-temperature-programmed reduction (H₂-TPR), UV–vis, X-ray absorption fine structure (XAFS), and in situ diffuse reflectance infrared Fourier transform spectroscopy (DRIFTS) methods. Based on the characterization results, the specific role of K doping in promoting the performance of Ag/Al₂O₃ was elucidated.

EXPERIMENTAL SECTION

Materials Preparation. The 8 wt % Ag/Al₂O₃ catalyst and K-8 wt % Ag/Al₂O₃ samples with different K doping quantities (0.5, 1, 2, and 4 wt %) were prepared by co-impregnation of Al₂O₃ (Aladdin, BET surface area 187.8 m²/g) with aqueous AgNO₃ and KNO₃ (Sigma-Aldrich). After stirring for 1 h, the excess water was removed in a rotary evaporator at 55 °C. Then, the samples were dried at 100 °C for 4 h and calcined at 450 °C for 3 h afterward. The samples were denoted as Ag/Al₂O₃ and 0.5–4K-Ag/Al₂O₃. The actual Ag and K contents in all the samples were measured using inductively coupled plasma optical emission spectrometry (OPTIMA 8300, PerkinElmer), and the data are presented in Table 1.

Material Characterization. The X-ray powder diffraction (XRD) patterns of the various catalysts were collected by an X-ray powder diffractometer (Bruker D8 ADVANCE Diffractometer) with Cu K α radiation ($\lambda = 0.15406$ nm) operated at 40 kV and 40 mA. The patterns were measured over the 2θ range from 5 to 80° with a scanning step of 0.02°.

Nitrogen adsorption–desorption isotherms were measured using a Quantachrome Quadrasorb SI-MP analyzer. The specific surface area of the samples was calculated by the Brunauer–Emmett–Teller (BET) method. The diameter and volume of the pores were determined by the Barrett–Joyner–Halenda method from the desorption branches of the isotherms.

High-resolution transmission electron microscopy (HR-TEM) images were obtained on a JEOL JEM 2010 TEM with 200 kV acceleration voltage. UV–vis measurements were

performed on a UV–vis spectrophotometer (Hitachi, U3100, Japan) using Al₂O₃ as a reference for the baseline spectrum.

The XANES of Ag–K edges were measured on beamline BL14W1 at the Shanghai Synchrotron Radiation Facility (SSRF). Ag foil and AgNO₃ were used as references. XANES spectra were normalized with the edge height to compare the variation in the absorption edge energies.

H₂ temperature-programmed reduction (H₂-TPR) was performed in a Micromeritics AutoChem II 2920 apparatus equipped with a computer-controlled CryoCooler and a thermal conductivity detector. The reduction profiles were obtained by passing a flow of 10% H₂/Ar at a rate of 50 mL/min (STP) through the sample (weight around 80 mg). The temperature was increased from 30 to 300 °C at the rate of 10 °C/min.

Activity Test for HCHO Oxidation. The activity tests for the catalytic oxidation of HCHO over the catalysts (60 mg) were performed in a fixed-bed quartz flow reactor (i.d. = 4 mm) in an incubator. Gaseous HCHO was generated by flowing helium through a paraformaldehyde container in a water bath kept at 35 °C. Water vapor was generated by flowing helium through a water bubbler at 25 °C and the water content was constant at varying temperatures of the experiments. The feed gas composition was 110 ppm of HCHO, 20% O₂, and balanced by helium, with or without 35% relative humidity (RH) at 25 °C. The total flow rate was 100 mL/min, corresponding to a gas hourly space velocity (GHSV) of 100 000 mL/(g_{cat} h). As with our previous instruments and methods to evaluate activity,^{22,40} the inlet and outlet gases were monitored by an FTIR spectrometer (Nicolet 380) equipped with 2 m gas cell and a deuterated triglycine sulfate detector; resolution: 0.5 cm⁻¹; optical path difference velocity: 0.4747 cm/s. The collection region was 4000–600 cm⁻¹ and the number of scans per spectrum was 16. HCHO and CO₂ were measured by the peaks located at 2897 (C–H vibration) and 2350 cm⁻¹ (O–C–O vibration), respectively. The inlet HCHO concentration was indirectly determined by measuring the concentration of CO₂ converted from HCHO. Specifically, the flow of He + HCHO + O₂ was first passed through a highly active catalyst such as Na–Pt/TiO₂, over which HCHO could be completely converted into CO₂ + H₂O. Next, we measured the CO₂ concentration and calculated the HCHO concentration. Before the measurement, a CO₂ standard curve was created using the different CO₂ concentrations vs the peak areas at 2350 cm⁻¹. As shown in our previous work,²² the CO₂ concentration below 500 ppm is a linear function of the IR peak area at 2350 cm⁻¹, which ensures that the measurements of the CO₂ and HCHO concentration are accurate.

RESULTS

Activity Test. Figure 1 shows the catalytic performance of various catalysts for HCHO oxidation. From Figure 1A, 100%

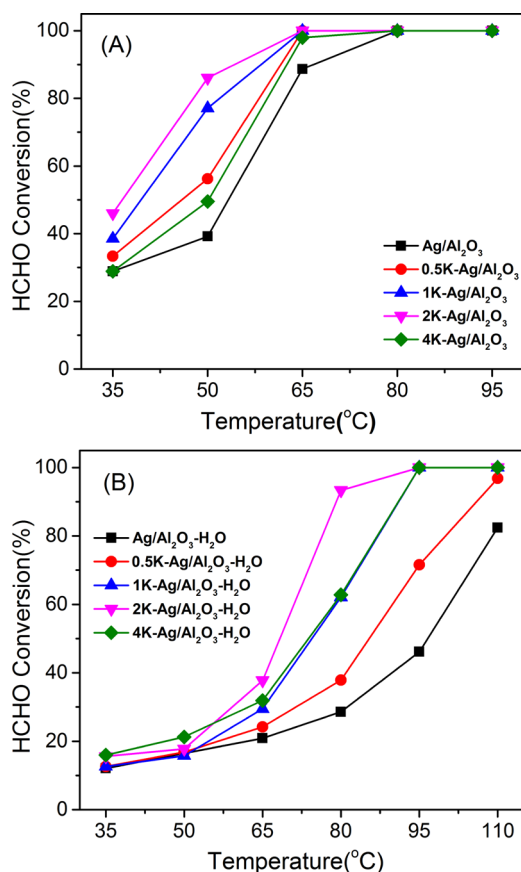


Figure 1. HCHO conversion over Ag/Al₂O₃ catalyst and K-doped Ag/Al₂O₃ catalysts without (A) and with (B) relative humidity (RH) at different temperatures. Reaction conditions: 110 ppm of HCHO, 20% O₂, 0% (A) or 35% (B) RH at 25 °C, He balance, and GHSV 100 000 mL/(g_{cat} h).

HCHO conversion was obtained at 80 °C for the Ag/Al₂O₃ catalyst at the space velocity of GHSV = 100 000 mL/(g_{cat} h). Remarkably, K addition led to a dramatic promotion effect on the Ag/Al₂O₃ catalyst. When the theoretical doping amount of K reached 2%, the 2K–Ag/Al₂O₃ catalyst showed the best low-temperature activity and completely oxidized HCHO at 65 °C. Further increasing the K content to 4 wt %, on the contrary, decreased the HCHO conversion in the low-temperature range. Thus, we can understand that K doping could improve the activity of Ag/Al₂O₃ catalyst for the catalytic oxidation of HCHO, but there was an optimal doping amount. In addition, we also tested the activity of the catalysts in the presence of water vapor. As shown in Figure 1B, when the RH was 35%, the activities of all the catalysts for HCHO oxidation clearly dropped off, indicating that water vapor had a negative effect on the catalytic performance in HCHO elimination, which should be due to the competitive adsorption of HCHO and H₂O.

Structural Features of Catalysts. XRD measurements were carried out to investigate the crystalline structures of the samples. As shown in Figure 2, the XRD pattern of the Ag/Al₂O₃ catalyst only exhibited the diffraction peaks of the γ -Al₂O₃ (JCPDS 74-2206) support and no Ag species (Ag⁰, Ag₂O), indicating that the Ag species were well dispersed on the γ -Al₂O₃ support. When K⁺ ions were doped on the Ag/Al₂O₃ catalyst, the (111), (200), (220), and (311) reflections of crystalline Ag (PDF no. 65-2871), corresponding to 38.1,

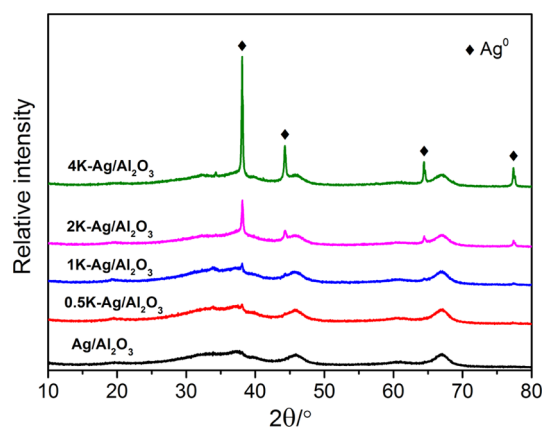


Figure 2. XRD patterns of Ag/Al₂O₃ catalyst and K-doped Ag/Al₂O₃ catalysts.

44.3, 64.4, and 77.5° (2 θ), respectively, were observed, and the intensities of the Ag diffraction peaks for K–Ag/Al₂O₃ were gradually augmented with the increase in the amount of K⁺ ions. The results indicated that the addition of K⁺ ions increased the crystallinity of Ag and decreased its dispersion.

BET measurements were next conducted to examine the physical properties of the samples. The specific surface area, pore size, and pore volume data are summarized in Table 1. The surface area and pore volume of the Ag/Al₂O₃ catalyst decreased with the addition of Ag compared to the pure γ -Al₂O₃ support, whereas the pore diameter basically remained the same. When K⁺ ions were added to the Ag/Al₂O₃ catalyst, all K-doped Ag/Al₂O₃ catalysts showed surface area, pore volume, and pore diameter similar to the Ag/Al₂O₃ catalyst, indicating that K doping had limited influence on these physical properties.

We next implemented TEM and HR-TEM measurements to investigate the morphology and particle size distribution of Ag over the catalysts. Figure 3a–e presents the TEM images of the respective samples, and the histograms inserted are the statistic results from 200 particles, and Figure 3f–j shows the HR-TEM images of the samples. In addition, we made a visual diagram (Figure 3k) of the change in the average Ag particle size with the increase in the K⁺ ion doping. As shown in Figure 3a, the Ag particles on the Ag/Al₂O₃ catalyst displayed a concentrated distribution ranging from 2 to 4 nm, with an average diameter of 3.5 nm. After K⁺ ions were doped into the Ag/Al₂O₃ catalyst, the particle sizes of the Ag nanoparticles increased,²⁶ and higher K⁺ doping resulted in larger Ag particle size. For the 4K–Ag/Al₂O₃ catalyst (Figure 3e), the average particle size of Ag species even reached 8.2 nm. According to previous studies,⁴¹ alkali ions can migrate into the lattice of Ag and change its crystal structure. We therefore speculated that the embedding of K ions in the Ag lattice weakened the interaction between Ag and the Al₂O₃ support, resulting in the decomposition of Ag into a metallic state and its aggregation into larger particles. As shown in Figure 3f–j, all the Ag/Al₂O₃ and K–Ag/Al₂O₃ samples exhibited more than one crystal face of Ag, such as Ag(111) and Ag(200) faces, with the lattice spacings of 0.236 and 0.204 nm, respectively. As reported by Bai et al.,²⁶ the addition of K⁺ ions could promote the exposure of Ag(111) planes. However, according to our results, the exposed Ag crystal faces were in a mixed crystal state, and the specific proportion of each crystal face could not be determined.

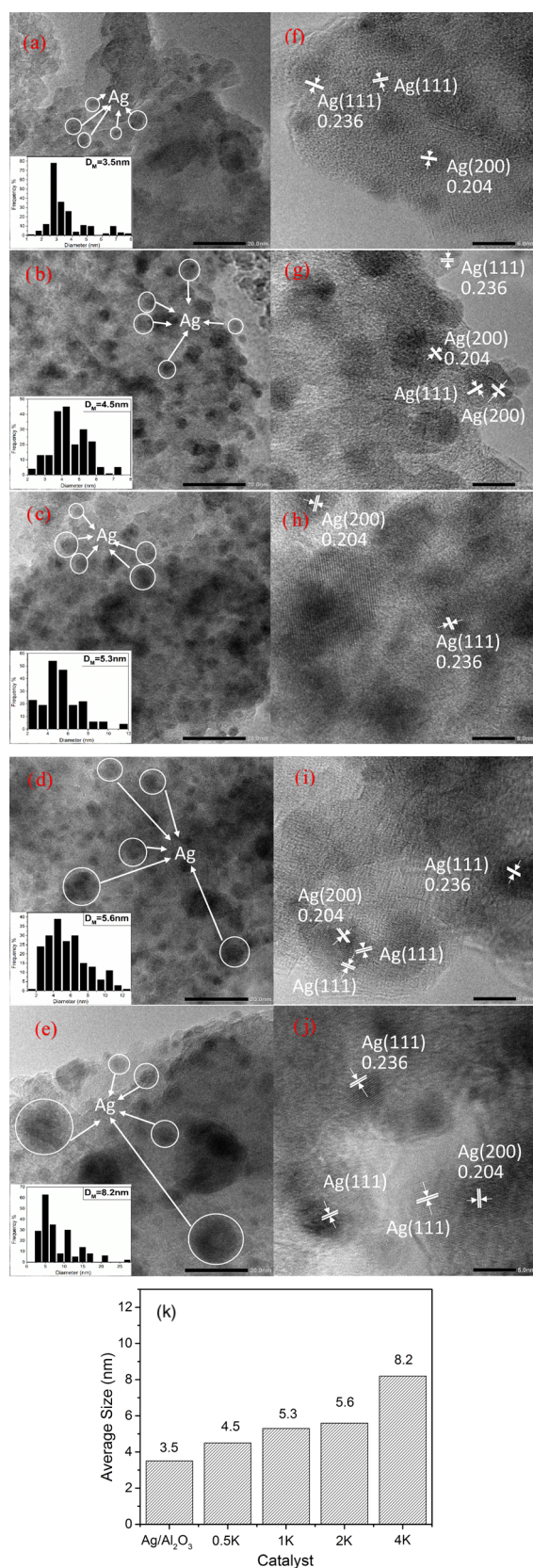


Figure 3. TEM and high-resolution TEM images of Ag/Al₂O₃ (a, f), 0.5% K-Ag/Al₂O₃ (b, g), 1% K-Ag/Al₂O₃ (c, h), 2% K-Ag/Al₂O₃ (d, i), and 4% K-Ag/Al₂O₃ (e, j) catalysts and summary of the average particle sizes of the samples (k).

Chemical Characterization of Catalysts. To understand the chemical state of supported Ag species, the Ag–K XANES of Ag/Al₂O₃ and K–Ag/Al₂O₃ catalysts, AgNO₃, and Ag foil were measured. According to the position of the white line in **Figure 4**, we can clearly see that the Ag–K absorption edges of

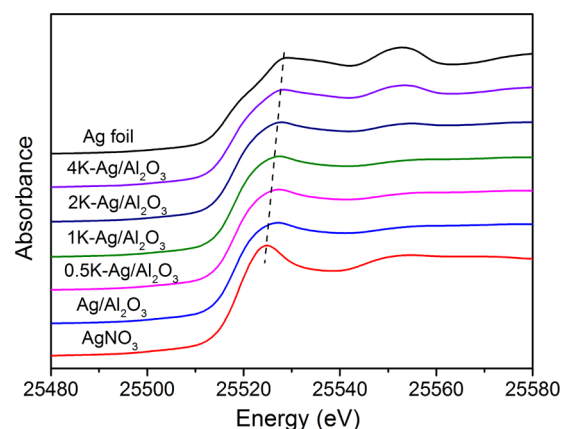


Figure 4. Normalized Ag–K XANES for Ag/Al₂O₃ catalyst and K-doped Ag/Al₂O₃ catalysts.

all the samples were located between those of Ag foil and AgNO₃, indicating that all catalyst samples exhibited both partial metallic state and partially oxidized state. In addition, it can clearly be seen that the absorption edges became gradually closer to the edge of Ag foil with increasing K doping, showing the increasing content of the metallic state. To prove this more convincingly, we further performed (linear combination) LC-XANES fits for the samples to determine the contents of Ag species with different valences. After performing principal-component analysis, we chose Ag foil and Ag₂O as model compounds, and the fitting results are summarized in **Table 2**.

Table 2. LC-XANES Fits of Ag–K in Ag/Al₂O₃ and K-Doped Ag/Al₂O₃ Catalysts

samples	Ag ⁰ (%)	Ag ⁺ (%)
Ag/Al ₂ O ₃	18.2	81.8
0.5K–Ag/Al ₂ O ₃	20.7	79.3
1K–Ag/Al ₂ O ₃	21.1	78.9
2K–Ag/Al ₂ O ₃	32.8	67.2
4K–Ag/Al ₂ O ₃	60.3	39.7

When the potassium ion doping level was 0, 0.5, 1, 2, and 4 wt %, the corresponding proportions of metallic silver in these sample were 18.2, 20.7, 21.1, 32.8, and 60.3%, respectively. The results showed that the content of metallic Ag was markedly increased with the addition of K⁺ ions, which was in agreement with the normalized data.

UV–vis measurement was also carried out to further investigate the details of the state of supported Ag, and the results are presented in **Figure 5**. According to previous studies,^{42–44} the absorption band around 210–220 nm was assigned to the 4d¹⁰ to 4d⁹5s¹ transition of Ag⁺ ions isolated on the support surface. In addition, the absorption band at ca. 270–320 nm should be ascribed to the small-charged Ag_{*n*}^{δ+} clusters, whereas the broad shoulder around 380 nm corresponded to the metallic Ag_{*n*}⁰ species, respectively. The peak intensity of Ag_{*n*}⁰ was enhanced with the increase in the K doping amount, apart from the 4K–Ag/Al₂O₃ catalyst. As seen

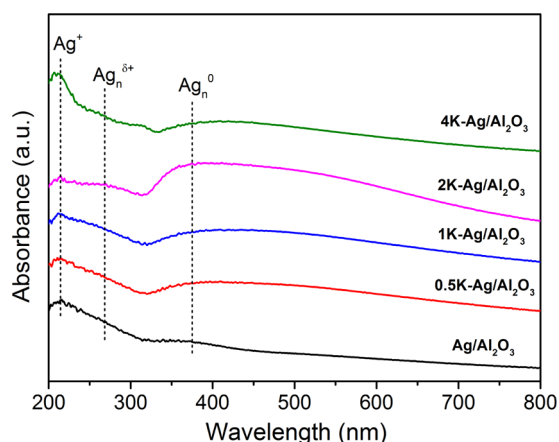


Figure 5. Diffuse-reflectance UV-vis spectra of $\text{Ag}/\text{Al}_2\text{O}_3$ catalyst and K-doped $\text{Ag}/\text{Al}_2\text{O}_3$ catalysts.

from the TEM images, the 4K- $\text{Ag}/\text{Al}_2\text{O}_3$ catalyst contains the largest Ag particles; therefore, the agglomeration of Ag decreased the exposure of metallic Ag on the catalyst surface, resulting in a decrease in the Ag_n^0 peak intensity in the 4K- $\text{Ag}/\text{Al}_2\text{O}_3$ sample. On the basis of the UV-vis results, we further concluded that the content of metallic Ag was increased due to the addition of K^+ ions, which was consistent with the results of XAFS.

Reducibility of Catalysts. H_2 -TPR was conducted to study the reducibility of the catalysts, and the TPR profiles of $\text{Ag}/\text{Al}_2\text{O}_3$ and K-doped $\text{Ag}/\text{Al}_2\text{O}_3$ catalysts are shown in Figure 6. The profile of the $\text{Ag}/\text{Al}_2\text{O}_3$ sample showed only one

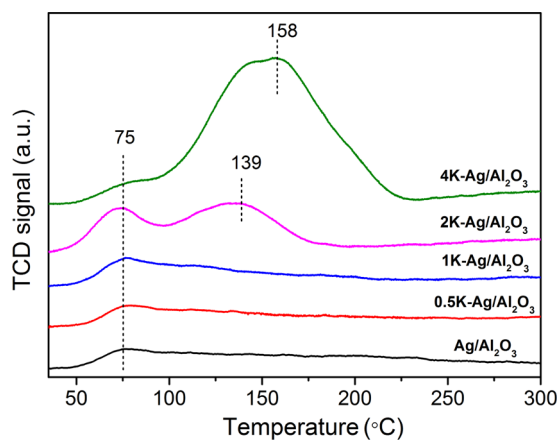


Figure 6. H_2 -TPR profiles of $\text{Ag}/\text{Al}_2\text{O}_3$ catalyst and K-doped $\text{Ag}/\text{Al}_2\text{O}_3$ catalysts.

reduction peak at 75 °C, which should be ascribed to the reduction of oxygen species adsorbed on the surface with dispersed metallic Ag.²⁷ Similarly, the peak located at around 75 °C appeared on all K- $\text{Ag}/\text{Al}_2\text{O}_3$ catalysts. The H_2 consumptions related to the reduction peaks at around 75 °C were quantified and the results are shown in Table 3. The H_2 consumption amount was increased with K^+ doping from 0.5 to 2%, indicating that the presence of K^+ ions increased the amount of oxygen species adsorbed on metallic Ag sites in $\text{Ag}/\text{Al}_2\text{O}_3$ catalysts. We believe that this promotion effect can be ascribed to the following two aspects. First, as reported by Ghosh et al.,⁴⁵ the supported metallic Ag nanoparticles could activate molecular oxygen and then catalyze the oxidation

Table 3. H_2 Consumption of $\text{Ag}/\text{Al}_2\text{O}_3$ and K-Doped $\text{Ag}/\text{Al}_2\text{O}_3$ Catalysts in H_2 -TPR at 75 °C

samples	H_2 consumption in H_2 -TPR at 75 °C ($\mu\text{mol}/\text{g}$)
$\text{Ag}/\text{Al}_2\text{O}_3$	24.1
0.5K- $\text{Ag}/\text{Al}_2\text{O}_3$	25.8
1K- $\text{Ag}/\text{Al}_2\text{O}_3$	34.3
2K- $\text{Ag}/\text{Al}_2\text{O}_3$	93.0
4K- $\text{Ag}/\text{Al}_2\text{O}_3$	28.1

reaction. We learned from the XAFS and UV-vis characterization results that the addition of K^+ ions increased the content of metallic Ag, therefore facilitating the adsorption and activation of oxygen. In accordance with the literature,⁴⁶ when oxygen is associatively chemisorbed on the Ag surface, partial charge transfer can be expected due to the overlap of the π^* -antibonding orbitals of O_2 with Ag orbitals. The added alkali metal ions partly covered the surface of Ag, and the resulting charge polarization at the surface changed the local electronic structure and status. This may enhance orbital coupling between O_2 and Ag, thus accounting for the increased adsorption and activation of O species. The addition of 4% K resulted in the obvious drop of H_2 consumption amount at around 75 °C, which is due to the loss of Ag sites by Ag aggregation. In addition, for 2K- $\text{Ag}/\text{Al}_2\text{O}_3$ and 4K- $\text{Ag}/\text{Al}_2\text{O}_3$ catalysts, another reduction peak respectively located at 139 and 158 °C should be assigned to the reduction of K species.

In Situ DRIFTS Study. The reaction mechanism of HCHO oxidation on $\text{Ag}/\text{Al}_2\text{O}_3$ and 2K- $\text{Ag}/\text{Al}_2\text{O}_3$ catalysts was next investigated at 50 °C by using in situ DRIFTS. The labels of 0.075, 0.015, and 0.3 in Figures 7 and 8 are the scales that represent the signal strength in the spectra. We used the different scales for better understanding the changes in peak intensities at different locations.

As shown in Figure 7A, when the $\text{Ag}/\text{Al}_2\text{O}_3$ catalyst was exposed to a flow of $\text{HCHO} + \text{O}_2 + \text{He}$, bands at 1342, 1377, 1395, 1595, 1630, 2120, 2746, 2828, 2861, 2891, and 3703 appeared. According to previous studies,^{19,26,40,47} we ascribed the bands at 1342, 1377, and 1395 to the symmetric stretch ν_s (COO^-) and those at 1595 and 1630 cm^{-1} to the asymmetric stretch ν_{as} (COO^-) of formate species. The bands near 1377 and 1595 cm^{-1} were related to the formate adsorbed on Al_2O_3 support. The peaks at 1395 and 1630 cm^{-1} were associated with the formate adsorbed on Ag sites, which was confirmed by density functional theory calculation results (insert in Figure 7A) showing that the COO asymmetric stretching vibration frequency on the Ag site was calculated as 1612 cm^{-1} . The bands at 2746, 2828, 2861, and 2891 cm^{-1} were ascribed to $\nu(\text{C-H})$. With increasing time, formate species were formed and increased. Meanwhile, a negative peak of surface hydroxyl (OH) species at 3703 cm^{-1} was observed on the catalyst surface, suggesting that the formation of surface HCOO^- consumed some OH species. In addition, a very weak band appearing at 2120 cm^{-1} is attributed to the CO species adsorbed on Ag. There was no peak associated with molecularly adsorbed HCOOH or HCHO on the $\text{Ag}/\text{Al}_2\text{O}_3$ catalyst, indicating that the adsorbed HCHO was rapidly converted to formate species in the flow of $\text{HCHO} + \text{O}_2 + \text{He}$.

After the $\text{Ag}/\text{Al}_2\text{O}_3$ catalyst was exposed to a flow of $\text{HCHO} + \text{O}_2 + \text{He}$ for 60 min, the sample was purged by He, and the corresponding changes are displayed as a function of time in Figure 7B. As can be seen, the bands of formate species decreased with increase in purging time. At the same time, the

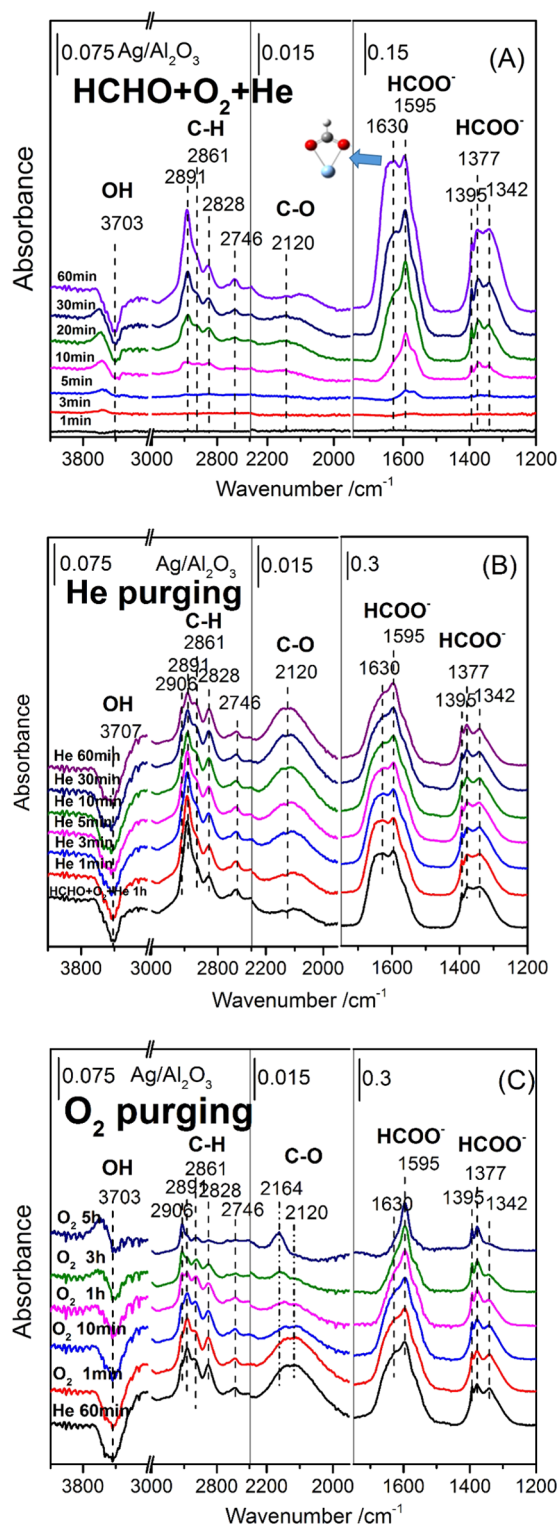


Figure 7. Dynamic changes of in situ DRIFTS for the Ag/Al₂O₃ catalyst as a function of time in a flow of (A) O₂ + HCHO + He. (B) He after exposing the catalyst to a flow of HCHO + O₂ + He. (C) O₂ after the sample was purged by He at 50 °C. Reaction conditions: 110 ppm of HCHO, 20% O₂, He balance, and total flow rate of 100 cm³/min. (The inset in (A) is the optimized configuration of HCOO interacting with the Ag site. Red, gray, white, and blue circles denote O, C, H, and Ag atoms, respectively. The theoretical vibrational frequencies were calculated using the 6-31G(d) basis set for the H, C, and O atoms, and the SDD pseudopotential and basis set for the Ag atom with B3LYP functional. The HCOO binds to the Ag site in a

Figure 7. continued

bidentate configuration. The calculated Ag–O distance is 2.31 Å. The C–O asymmetric stretching vibration frequency is 1612 cm⁻¹.)

intensity of the band at 2120 cm⁻¹ due to adsorbed CO increased and the peak associated with surface hydroxyl (OH) species at 3703 cm⁻¹ basically remained unchanged. Taking these results into account, we believe that the surface formate species decomposed to form adsorbed CO at 50 °C in the absence of O₂. As shown in Figure 7C, upon exposure of the catalyst to O₂, the formate species (2746, 2828, 2861, 2891, 1342, 1377, 1395, 1595, and 1630 cm⁻¹) and CO (2120 cm⁻¹) adsorbed on the Ag/Al₂O₃ catalyst decreased gradually, demonstrating that the surface formate species decomposed into adsorbed CO species, and the CO species finally reacted with O₂ to produce CO₂. After oxygen purging for 5 h, there was a small peak still remaining at the position of formate species. This may be due to the relative low reactivity of formate species with O₂ at this low temperature. Another possibility is that the small peak might be related to the carbonate or bicarbonate species because there are some overlap among IR peaks of formate, carbonate, and bicarbonate species. In addition, the band at 2164 cm⁻¹ was also ascribed to the CO species adsorbed on different sites of Ag/Al₂O₃. As we can see from Figures 7C and 8C, after the system was exposed to O₂, the adsorbed formate species on the catalysts were consumed and accordingly the peaks decreased gradually; therefore, some new sites would be available for CO adsorption. The reactivity of adsorbed CO at 2164 cm⁻¹ should be relatively low, thus it built up with time.

We performed the same in situ DRIFTS experiments over the 2K–Ag/Al₂O₃ catalyst and observed a similar reaction route for HCHO oxidation (shown in Figure 8). HCHO first adsorbed on the Al₂O₃ and Ag sites to form formate species. Subsequently, the formate species was decomposed into CO (2090 cm⁻¹) with He purging, and the CO species finally reacted with O₂ to produce CO₂. Therefore, it was concluded that the HCHO oxidation reaction on Ag/Al₂O₃ and 2K–Ag/Al₂O₃ samples followed the same mechanism of HCHO → HCOO⁻ → CO → CO₂.

Furthermore, we integrated the band areas of the formate species (1595 and 1630 cm⁻¹) in Figures 7C and 8C, obtained the changes in the band areas with time, and finally calculated the rate of formate consumption on Ag/Al₂O₃ and 2K–Ag/Al₂O₃ catalysts with exposure to O₂. As shown in Figure 9, in the first 30 min, the reduction in the formate band area on the 2K–Ag/Al₂O₃ catalyst was much faster than on that on the Ag/Al₂O₃ catalyst, and the corresponding slopes were -1.97 and -1.44, respectively. Clearly, HCHO was consumed more rapidly on the 2K–Ag/Al₂O₃ catalyst even though the mechanism of HCHO oxidation for the Ag/Al₂O₃ catalysts did not change with the addition of K species, indicating that the 2K–Ag/Al₂O₃ catalyst had a stronger capability for O₂ activation, confirming the conclusion of the H₂-TPR results.

DISCUSSION

The activity test results showed that K species doping greatly improved the activity of Ag/Al₂O₃ catalysts for catalytic oxidation of HCHO in the absence of water vapor. However, when the RH was 35%, the activities of all the catalysts for HCHO oxidation were severely suppressed whether or not K

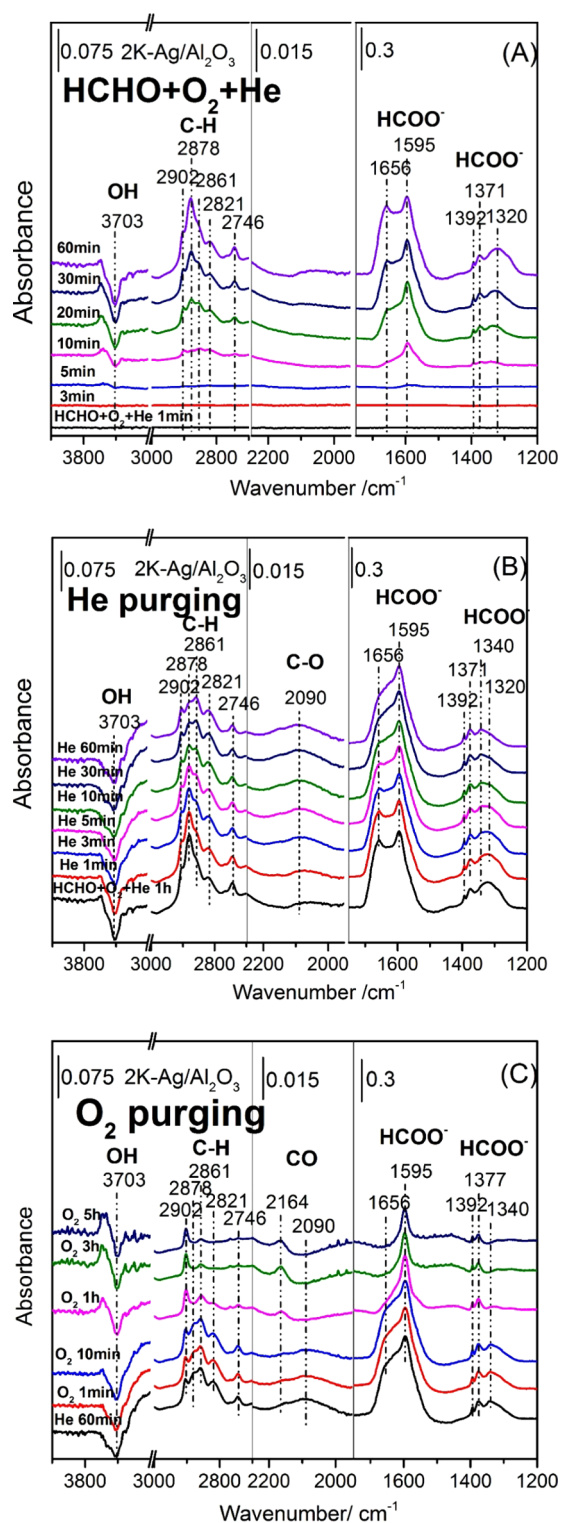


Figure 8. Dynamic changes in in situ DRIFTS of the 2K-Ag/Al₂O₃ catalyst as a function of time in a flow of (A) O₂ + HCHO + He. (B) He after exposing catalyst to a flow of HCHO + O₂ + He. (C) O₂ after the sample was purged by He at 50 °C. Reaction conditions: 110 ppm of HCHO, 20% O₂, He balance, and total flow rate of 100 cm³/min.

was added. Our previous studies showed that HCHO oxidation could be greatly promoted by water vapor on Pt- and Pd-based catalysts.^{40,48} This indicated that the adsorbed H₂O on Pt and Pd catalysts could be activated to form surface

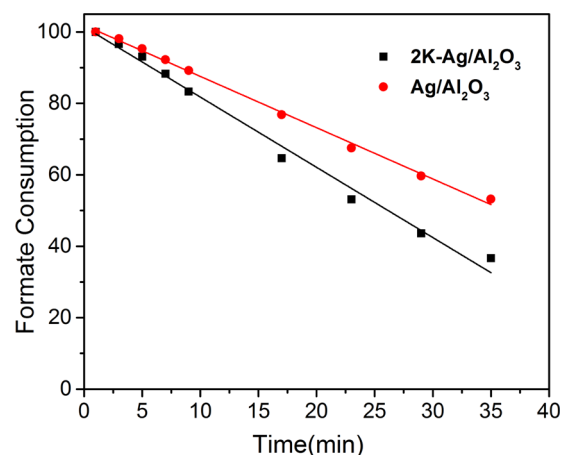


Figure 9. Changes in the band areas of the formate species (1595, 1630 or 1595, 1656 cm⁻¹) over time on Ag/Al₂O₃ and 2K-Ag/Al₂O₃ catalysts with exposure to O₂.

OH groups participating in the direct oxidation of formate, and alkali ion addition could promote the H₂O activation, therefore enhancing the activity. In this study, we observed that water vapor inhibited the activities of both the Ag/Al₂O₃ and K-Ag/Al₂O₃ catalysts, indicating that the Ag species is not capable of H₂O activation in the low-temperature range even with K doping. The decrease in catalytic performance should be due to the competitive adsorption of water on the catalyst surface.

The XAFS and UV-vis results showed that the content of metallic Ag species was increased when the Ag/Al₂O₃ catalyst was doped with K⁺ ions. As was previously reported, the metallic Ag species is a more active site than Ag oxide for the adsorption and activation of oxygen species at low temperatures; therefore, more metallic Ag species will be beneficial to the catalytic performance. As shown from the H₂-TPR results and the test results, the 2K-Ag/Al₂O₃ catalyst has the highest redox ability among all catalysts and also demonstrates the highest activity for HCHO oxidation, indicating that the promotion of O₂ activation by K doping is the key factor in improving the catalytic performance.

The XRD and TEM results showed that K addition also led to the enlargement of Ag particles, and the higher the K doping amount, the larger the Ag particles were. Because the Ag particles were severely aggregated on the 4K-Ag/Al₂O₃ catalyst, resulting in the loss of active Ag sites, the 4K-Ag/Al₂O₃ catalyst demonstrated a much lower performance than 2K-Ag/Al₂O₃. Bai et al.²⁶ previously reported that Ag(111) planes are the most active faces for HCHO oxidation and that K doping could favor the exposure of more Ag(111) crystal faces, which is beneficial to the catalytic oxidation of HCHO. However, our HR-TEM results showed that the exposed crystal surface of Ag in all the samples existed in a mixed crystal state, and the specific proportion of each crystal plane could not be determined. Therefore, it is not clear whether the catalytic oxidation activity of HCHO was related to the activity of the Ag(111) crystallographic plane. Nevertheless, the addition of Ag K⁺ ions did not change the reaction mechanism of the Ag/Al₂O₃ catalysts.

CONCLUSIONS

In summary, this work demonstrated that K addition had a dramatic promotion effect on Ag/Al₂O₃ catalysts for HCHO oxidation, and the 2K-Ag/Al₂O₃ sample showed the highest

activity, achieving the complete conversion of HCHO into CO₂ and H₂O at 65 °C in a GHSV of 100 000 mL/(g_{cat} h). The addition of K⁺ ions greatly increased the content of metallic Ag species in the Ag/Al₂O₃ catalysts, promoting the adsorption and activation of oxygen species, which is the key factor in the improved catalytic performance. Nevertheless, K could penetrate the Ag lattice due to their similar atomic sizes, resulting in the structural rearrangement of Ag and leading to the agglomeration and the loss of active Ag sites when excessive K⁺ was added. The addition of K⁺ ions did not change the reaction mechanism of the Ag/Al₂O₃ catalysts. HCHO oxidation on Ag/Al₂O₃ and 2K–Ag/Al₂O₃ samples followed the same pathway of HCHO → HCOO[−] → CO → CO₂.

AUTHOR INFORMATION

Corresponding Author

*E-mail: cbzhang@rcees.ac.cn. Tel/Fax: (+86) 10 62849121.

ORCID

Guangzhi He: 0000-0003-1770-3522

Fei Wang: 0000-0002-4364-9956

Guangyan Xu: 0000-0002-4275-7517

Changbin Zhang: 0000-0003-2124-0620

Notes

The authors declare no competing financial interest.

ACKNOWLEDGMENTS

This work was financially supported by the National Key R&D Program of China (2017YFC0211802), the National Natural Science Foundation of China (21577159), and the Key Research Program of Frontier Sciences, CAS (QYZDB-SSW-DQC018).

REFERENCES

- (1) Yu, C.; Crump, D. A Review of the Emission of VOCs from Polymeric Materials Used in Buildings. *Build. Environ.* **1998**, *33*, 357–374.
- (2) Collins, J. J.; Ness, R.; Tyl, R. W.; Krivanek, N.; Esmen, N. A.; Hall, T. A. A Review of Adverse Pregnancy Outcomes and Formaldehyde Exposure in Human and Animal Studies. *Regul. Toxicol. Pharmacol.* **2001**, *34*, 17–34.
- (3) Jones, A. P. Indoor Air Quality and Health. *Atmos. Environ.* **1999**, *33*, 4535–4564.
- (4) Nie, L.; Yu, J.; Jaroniec, M.; Tao, F. F. Room-Temperature Catalytic Oxidation of Formaldehyde on Catalysts. *Catal. Sci. Technol.* **2016**, *6*, 3649–3669.
- (5) Rong, H.; Liu, Z.; Wu, Q.; Pan, D.; Zheng, J. Formaldehyde Removal by Rayon-based Activated Carbon Fibers Modified by P-Aminobenzoic Acid. *Cellulose* **2010**, *17*, 205–214.
- (6) Noguchi, T.; Fujishima, A.; Sawunyama, P.; Hashimoto, K. Photocatalytic Degradation of Gaseous Formaldehyde Using TiO₂ Film. *Environ. Sci. Technol.* **1998**, *32*, 3831–3833.
- (7) Ye, J.; Zhu, X.; Cheng, B.; Yu, J.; Jiang, C. Few-Layered Graphene-like Boron Nitride: A Highly Efficient Adsorbent for Indoor Formaldehyde Removal. *Environ. Sci. Tech. Lett.* **2017**, *4*, 20–25.
- (8) Zhu, X.; Gao, X.; Qin, R.; Zeng, Y.; Qu, R.; Zheng, C.; Tu, X. Plasma-catalytic Removal of Formaldehyde over Cu–Ce Catalysts in a Dielectric Barrier Discharge Reactor. *Appl. Catal., B* **2015**, *170–171*, 293–300.
- (9) Bai, B.; Qiao, Q.; Li, J.; Hao, J. Progress in Research on Catalysts for Catalytic Oxidation of Formaldehyde. *Chin. J. Catal.* **2016**, *37*, 102–122.
- (10) Quiroz Torres, J.; Royer, S.; Bellat, J.-P.; Giraudon, J.-M.; Lamonnier, J.-F. Formaldehyde: Catalytic Oxidation as a Promising Soft Way of Elimination. *ChemSusChem* **2013**, *6*, 578–592.
- (11) Bai, B.; Arandiyan, H.; Li, J. Comparison of the Performance for Oxidation of Formaldehyde on Nano-Co₃O₄, 2D-Co₃O₄, and 3D-Co₃O₄ Catalysts. *Appl. Catal., B* **2013**, *142–143*, 677–683.
- (12) Qu, Z.; Sun, Y.; Chen, D.; Wang, Y. Possible Sites of Copper Located on Hydroxyapatite Structure and the Identification of Active Sites for Formaldehyde Oxidation. *J. Mol. Catal. A: Chem.* **2014**, *393*, 182–190.
- (13) Huang, Y.; Long, B.; Tang, M.; Rui, Z.; Balogun, M.-S.; Tong, Y.; Ji, H. Bifunctional Catalytic Material: An Ultrastable and High-Performance Surface Defect CeO₂ Nanosheets for Formaldehyde Thermal Oxidation and Photocatalytic Oxidation. *Appl. Catal., B* **2016**, *181*, 779–787.
- (14) Wang, Y.; Zhu, X.; Crocker, M.; Chen, B.; Shi, C. A Comparative Study of the Catalytic Oxidation of HCHO and CO over Mn_{0.75}Co_{2.25}O₄ Catalyst: The Effect of Moisture. *Appl. Catal., B* **2014**, *160–161*, 542–551.
- (15) Wang, J.; Li, J.; Jiang, C.; Zhou, P.; Zhang, P.; Yu, J. The Effect of Manganese Vacancy in Birnessite-type MnO₂ on Room-Temperature Oxidation of Formaldehyde in Air. *Appl. Catal., B* **2017**, *204*, 147–155.
- (16) Wang, Z.; Wang, W.; Zhang, L.; Jiang, D. Surface Oxygen Vacancies on Co₃O₄ Mediated Catalytic Formaldehyde Oxidation at Room Temperature. *Catal. Sci. Technol.* **2016**, *6*, 3845–3853.
- (17) Zhang, J.; Li, Y.; Wang, L.; Zhang, C.; He, H. Catalytic Oxidation of Formaldehyde over Manganese Oxides with Different Crystal Structures. *Catal. Sci. Technol.* **2015**, *5*, 2305–2313.
- (18) Zhang, C.; He, H.; Tanaka, K.-i. Perfect Catalytic Oxidation of Formaldehyde over a Pt/TiO₂ Catalyst at Room Temperature. *Catal. Commun.* **2005**, *6*, 211–214.
- (19) Zhang, C.; He, H.; Tanaka, K.-i. Catalytic Performance and Mechanism of a Pt/TiO₂ Catalyst for the Oxidation of Formaldehyde at Room Temperature. *Appl. Catal., B* **2006**, *65*, 37–43.
- (20) Tang, X.; Chen, J.; Huang, X.; Xu, Y.; Shen, W. Pt/MnO_x–CeO₂ Catalysts for the Complete Oxidation of Formaldehyde at Ambient Temperature. *Appl. Catal., B* **2008**, *81*, 115–121.
- (21) Nie, L.; Meng, A.; Yu, J.; Jaroniec, M. Hierarchically Macroporous Pt/γ-Al₂O₃ Composite Microspheres for Efficient Formaldehyde Oxidation at Room Temperature. *Sci. Rep.* **2013**, *3*, No. 3215.
- (22) Zhang, C.; Li, Y.; Wang, Y.; He, H. Sodium-Promoted Pd/TiO₂ for Catalytic Oxidation of Formaldehyde at Ambient Temperature. *Environ. Sci. Technol.* **2014**, *48*, 5816–5822.
- (23) Huang, H.; Leung, D. Y. C. Complete Oxidation of Formaldehyde at Room Temperature Using TiO₂ Supported Metallic Pd Nanoparticles. *ACS Catal.* **2011**, *1*, 348–354.
- (24) Liu, B.; Liu, Y.; Li, C.; Hu, W.; Jing, P.; Wang, Q.; Zhang, J. Three-dimensionally Ordered Macroporous Au/CeO₂–Co₃O₄ Catalysts with Nanoporous Walls for Enhanced Catalytic Oxidation of Formaldehyde. *Appl. Catal., B* **2012**, *127*, 47–58.
- (25) Huang, Z.; Gu, X.; Cao, Q.; Hu, P.; Hao, J.; Li, J.; Tang, X. Catalytically Active Single-Atom Sites Fabricated from Silver Particles. *Angew. Chem., Int. Ed.* **2012**, *124*, 4274–4279.
- (26) Bai, B.; Li, J. Positive Effects of K⁺ Ions on Three-Dimensional Mesoporous Ag/Co₃O₄ Catalyst for HCHO Oxidation. *ACS Catal.* **2014**, *4*, 2753–2762.
- (27) Zhang, J.; Li, Y.; Zhang, Y.; Chen, M.; Wang, L.; Zhang, C.; He, H. Effect of Support on the Activity of Ag-Based Catalysts for Formaldehyde Oxidation. *Sci. Rep.* **2015**, *5*, No. 12950.
- (28) Ma, L.; Wang, D.; Li, J.; Bai, B.; Fu, L.; Li, Y. Ag/CeO₂ Nanospheres: Efficient Catalysts for Formaldehyde Oxidation. *Appl. Catal., B* **2014**, *148*, 36–43.
- (29) Yan, Z.; Xu, Z.; Yu, J.; Jaroniec, M. Highly Active Mesoporous Ferrihydrite Supported Pt Catalyst for Formaldehyde Removal at Room Temperature. *Environ. Sci. Technol.* **2015**, *49*, 6637–6644.
- (30) Nie, L.; Yu, J.; Li, X.; Cheng, B.; Liu, G.; Jaroniec, M. Enhanced Performance of NaOH-Modified Pt/TiO₂ toward Room Temperature

Selective Oxidation of Formaldehyde. *Environ. Sci. Technol.* **2013**, *47*, 2777–2783.

(31) Tan, H.; Wang, J.; Yu, S.; Zhou, K. Support Morphology-Dependent Catalytic Activity of Pd/CeO₂ for Formaldehyde Oxidation. *Environ. Sci. Technol.* **2015**, *49*, 8675–8682.

(32) Ma, C.; Wang, D.; Xue, W.; Dou, B.; Wang, H.; Hao, Z. Investigation of Formaldehyde Oxidation over Co₃O₄–CeO₂ and Au/Co₃O₄–CeO₂ Catalysts at Room Temperature: Effective Removal and Determination of Reaction Mechanism. *Environ. Sci. Technol.* **2011**, *45*, 3628–3634.

(33) Xu, Q.; Lei, W.; Li, X.; Qi, X.; Yu, J.; Liu, G.; Wang, J.; Zhang, P. Efficient Removal of Formaldehyde by Nanosized Gold on Well-Defined CeO₂ Nanorods at Room Temperature. *Environ. Sci. Technol.* **2014**, *48*, 9702–9708.

(34) Bai, B.; Qiao, Q.; Arandiyani, H.; Li, J.; Hao, J. Three-Dimensional Ordered Mesoporous MnO₂-Supported Ag Nanoparticles for Catalytic Removal of Formaldehyde. *Environ. Sci. Technol.* **2016**, *50*, 2635–2640.

(35) Hu, P.; Amghouz, Z.; Huang, Z.; Xu, F.; Chen, Y.; Tang, X. Surface-Confined Atomic Silver Centers Catalyzing Formaldehyde Oxidation. *Environ. Sci. Technol.* **2015**, *49*, 2384–2390.

(36) Li, Y.; Zhang, C.; He, H.; Zhang, J.; Chen, M. Influence of Alkali Metals on Pd/TiO₂ Catalysts for Catalytic Oxidation of Formaldehyde at Room Temperature. *Catal. Sci. Technol.* **2016**, *6*, 2289–2295.

(37) Na, H.; Zhu, T.; Liu, Z. Effect of Preparation Method on the Performance of Pt–Au/TiO₂ Catalysts for the Catalytic co-Oxidation of HCHO and CO. *Catal. Sci. Technol.* **2014**, *4*, 2051.

(38) Qi, L.; Ho, W.; Wang, J.; Zhang, P.; Yu, J. Enhanced Catalytic Activity of Hierarchically Macro-/Mesoporous Pt/TiO₂ toward Room-Temperature Decomposition of Formaldehyde. *Catal. Sci. Technol.* **2015**, *5*, 2366–2377.

(39) Wang, X.; Rui, Z.; Ji, H. DFT Study of Formaldehyde Oxidation on Silver Cluster by Active Oxygen and Hydroxyl Groups: Mechanism Comparison and Synergistic Effect. *Catal. Today* **2018**, DOI: 10.1016/j.cattod.2018.06.021.

(40) Zhang, C.; Liu, F.; Zhai, Y.; Ariga, H.; Yi, N.; Liu, Y.; Asakura, K.; Flytzani-Stephanopoulos, M.; He, H. Alkali-Metal-Promoted Pt/TiO₂ Opens a More Efficient Pathway to Formaldehyde Oxidation at Ambient Temperatures. *Angew. Chem., Int. Ed.* **2012**, *51*, 9628–9632.

(41) Kitson, M.; Lambert, R. M. Basic Studies of the Oxygen Chemistry of Silver: Oxygen, Dioxide and Superoxide on Potassium-Dosed Ag(100). *Surf. Sci.* **1981**, *109*, 60–74.

(42) Shimizu, K.-i.; Shibata, J.; Yoshida, H.; Satsuma, A.; Hattori, T. Silver-Alumina Catalysts for Selective Reduction of NO by Higher Hydrocarbons: Structure of Active Sites and Reaction Mechanism. *Appl. Catal., B* **2001**, *30*, 151–162.

(43) Wagner, C. D. *Handbook of X-ray Photoelectron Spectroscopy*; Perkin-Elmer, 1979.

(44) Pestryakov, A. N.; Davydov, A. A. Active Electronic States of Silver Catalysts for Methanol Selective Oxidation. *Appl. Catal., A* **1994**, *120*, 7–15.

(45) Ghosh, S.; Acharyya, S. S.; Tiwari, R.; Sarkar, B.; Singha, R. K.; Pendem, C.; Sasaki, T.; Bal, R. Selective Oxidation of Propylene to Propylene Oxide over Silver-Supported Tungsten Oxide Nanostructure with Molecular Oxygen. *ACS Catal.* **2014**, *4*, 2169–2174.

(46) Garfunkel, E.; Xun-min, D.; et al. The Effect of Sodium Adlayers on the Adsorption of Oxygen on Ag(100). *Chin. Phys. Lett.* **1985**, *2*, 397.

(47) Shi, C.; Chen, B.; Li, X.; Crocker, M.; Wang, Y.; Zhu, A. Catalytic Formaldehyde Removal by “Storage-Oxidation” Cycling Process over Supported Silver Catalysts. *Chem. Eng. J.* **2012**, *200–202*, 729–737.

(48) Li, Y.; Zhang, C.; Ma, J.; Chen, M.; Deng, H.; He, H. High Temperature Reduction Dramatically Promotes Pd/TiO₂ Catalyst for Ambient Formaldehyde Oxidation. *Appl. Catal., B* **2017**, *217*, 560–569.